RSC Advances

PAPER

View Article Online
View Journal | View Issue

Cite this: *RSC Adv.*, 2020, **10**, 32216

TDDFT-ECD and DFT-NMR studies of thaigranatins A–E and granatumin L isolated from *Xylocarpus granatum*†

Attila Mándi,[a] Jun Wu*[b] and Tibor Kurtán*[a]

Received 25th April 2020
Accepted 20th August 2020

DOI: 10.1039/d0ra03725g

rsc.li/rsc-advances

TDDFT-ECD calculations were utilized to explain the mirror image or different ECD spectra of previously reported homochiral natural products thaigranatins A–E and granatumin L, the simple comparison of which would result in a wrong stereochemical conclusion. The configurational assignment was confirmed independently and geometrical parameters of the chromophores governing the ECD spectra were identified in the structurally related natural products by analyzing the ECD spectra and geometries of the low-energy computed conformers obtained by different methods. Different conformations of the furan-2-yl-δ-lactone subunit were found responsible for the mirror image ECD spectra of the homochiral thaigranatins C–E. Two DFT ^{13}C NMR chemical shift calculation methods and DP4+ analysis were performed on the C-6 epimers of thaigranatin D, which together with the ECD calculation, could determine the absolute configuration of C-6 as (*R*).

Introduction

Due to the low sample amount requirement and efficient reproduction of the experimental electronic circular dichroism (ECD) spectra by time-dependent density functional theory ECD (TDDFT-ECD) calculations, ECD is considered the most widely applied microscale chiroptical method for the configurational assignment of natural products (NPs) containing chromophores with absorbance in the UV-vis spectral range.[1–3] For structurally related NPs, the simple comparison of experimental ECD spectra is often utilized to determine the absolute configuration (AC) if it was determined for one of the derivatives. For instance, the C-3 AC of pseudoanguillosporin B (**C**), an isochroman derivative with a 6-hydroxyhept-1-yl side-chain at C-3, was determined by comparing the ECD spectrum with that of the co-isolated pseudoanguillosporin A (**B**) containing only a C-3 heptyl substituent (Fig. 1).[4] The remote C-6′ chirality center of **C** was far from the isochroman chromophore and it had practically no contribution to the ECD profile, which justified the comparison of the ECD spectra of **B** and **C**. The absolute configuration of **B** was confirmed by the solution TDDFT-ECD calculation approach applied for the truncated model compound **A**, containing only a C-3 methyl group.[4] Although chiroptical data of homochiral related derivatives are often similar, a subtle change in the planar structure or substitution pattern may result in rather different[5–8] or nearly opposite ECD spectra or optical rotation.[9–13] TDDFT-ECD calculations of structurally related NPs having markedly different ECD spectra were found useful to interpret the differences.

For instance, the pyridine alkaloids penipyridones C (**D**) and F (**E**) had the same chromophoric system and absolute configuration but **E** had an additional *N*-2-hydroxyethyl group, which resulted in near mirror image ECD spectra and oppositely signed specific rotation (Fig. 1).[10] TDDFT-ECD calculations and analysis of the low-energy conformers revealed that in the presence of the achiral *N*-2-hydroxyethyl substituent, the additional 15-OH group formed an intramolecular hydrogen bond with the 7-OH, which changed the relative orientation of the phenyl and γ-pyridone chromophores.[10] The replacement of oxygen heteroatom with sulfur in the benzene-condensed spiro derivatives **F** and **G** containing benzo[1,4]oxazin-3-one and benzo[1,4]thiazin-3-one chromophores resulted in significantly different ECD spectra with mirror image transitions in the high-wavelength region, although the computed conformers had very similar geometries (Fig. 1).[9]

Aflaquinolone I (**H**) and aniduquinolone A (**I**) shared a very similar substituted 4-aryl-3,4-dihydroquinolin-2(1*H*)-one chromophore but in the presence of the 5-OH group in the *peri* position of **I**, the C-4 phenyl group adopted an axial orientation, while in **H**, having a hydrogen atom in the *peri* position, the C-4 aryl group preferred the equatorial orientation in all the low-energy computed conformers (Fig. 1).[6,7] Due to the different conformations of the condensed heterocycles, the ECD spectra of **H** and **I** were fairly different and comparison of ECDs could not be used to determine the AC of **H**.[7] Psammaplysins A (**J**) and

[a]*Department of Organic Chemistry, University of Debrecen, P. O. Box 400, 4002 Debrecen, Hungary. E-mail: kurtan.tibor@science.unideb.hu; Fax: +36-52-512-744*
[b]*School of Pharmaceutical Sciences, Southern Medical University, 1838 Guangzhou Avenue North, Guangzhou 510515, P. R. China. E-mail: wwujun2003@yahoo.com*

† Electronic supplementary information (ESI) available. See DOI: 10.1039/d0ra03725g

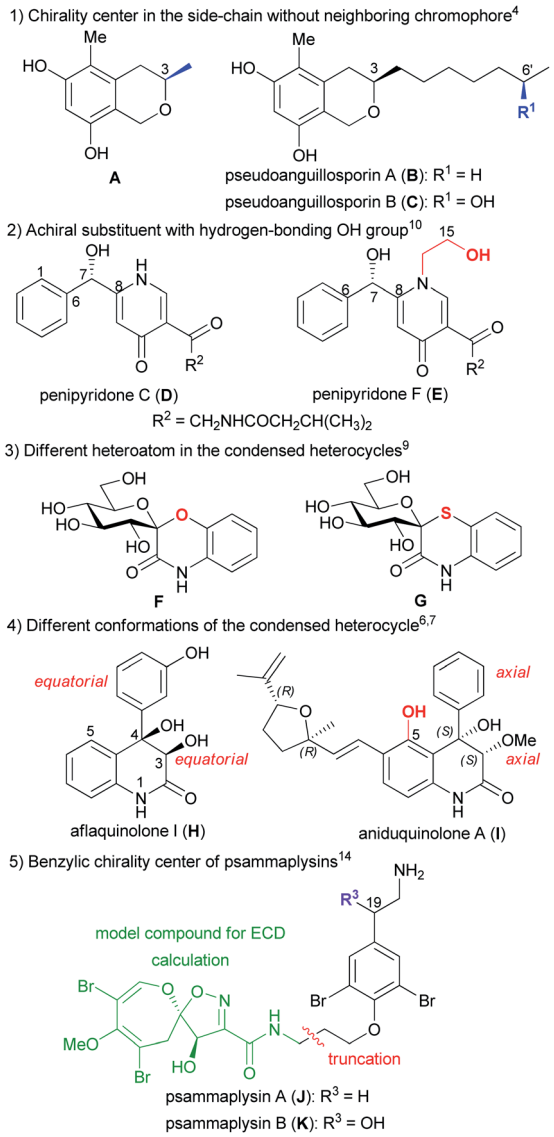

Fig. 1 Examples on the comparison of ECD spectra of structurally related derivatives.

B (**K**), first representatives of the psammaplysin alkaloid family, differed in the additional C-19 benzylic hydroxyl group of **K**, which implied a C-19 chirality center in the side-chain of **K** (Fig. 1).[14] Regardless this benzylic chirality center, the experimental ECD spectra of **J** and **K** were found near identical, which confirmed that the side-chain with an aryl ether chromophore had negligible contribution to the ECD spectra. Thus a truncated model compound could be utilized for the ECD calculations of **J**, which reduced the number of conformers and enabled the configurational assignment of **J**.[14] The above examples may justify to explore the structural and chiroptical background for the different ECD profiles of structurally related derivatives by ECD calculations, which would allow us avoiding wrong configurational assignments for analogous derivatives.

Thaigranatins A–E (**1–5**), limonoid derivatives containing a pentacyclic skeleton with a furan-3-yl substituent at the δ-lactone ring E, have been recently isolated together with the previously described granatumin L[15] (**6**) from the seeds of the Thai *Xylocarpus granatum* and reported by Ren *et al.* (Fig. 2).[16]

Related limonoids with the same skeleton have been isolated recently from *Xylocarpus granatum*,[17–20] *Xylocarpus moluccensis*,[21,22] *Chisocheton ceramicus*[23] and *Chisocheton erythrocarpus*.[24] Limonoids were suggested to have even potent inhibitory activity against SARS-CoV-2 by *in silico* docking studies.[25] Since limonoids exhibit a wide range of bioactivities such as antiviral, anticancer activity and they are potential endogenous regulators in the nervous system, they have also attracted considerable synthetic interest.[26]

The AC of thaigranatin A (**1**) was elucidated by single crystal X-ray analysis, while those of **2** and **6** were determined on the basis of their similar ECD spectra to that of thaigranatin A (**1**).[16] The experimental solution ECD spectra of **1** and **6** were quite similar, while that of **2** had a broad positive ECD band with a maximum at 217 nm, which were missing from those of **1** and **6**. The ECD spectra of **3–5** were significantly different from the others, which did not enable to utilize the simple comparison of the ECD spectra for the configurational assignment. Moreover, the ECD spectrum of **5** was found near mirror image of those of **3** and **4**, which is quite puzzling considering their analogous structure with minor structural differences (Fig. 3). The absolute configurations of **3–5** were proposed on the basis of the common biosynthetic origin with thaigranatin A (**1**).[16] In this

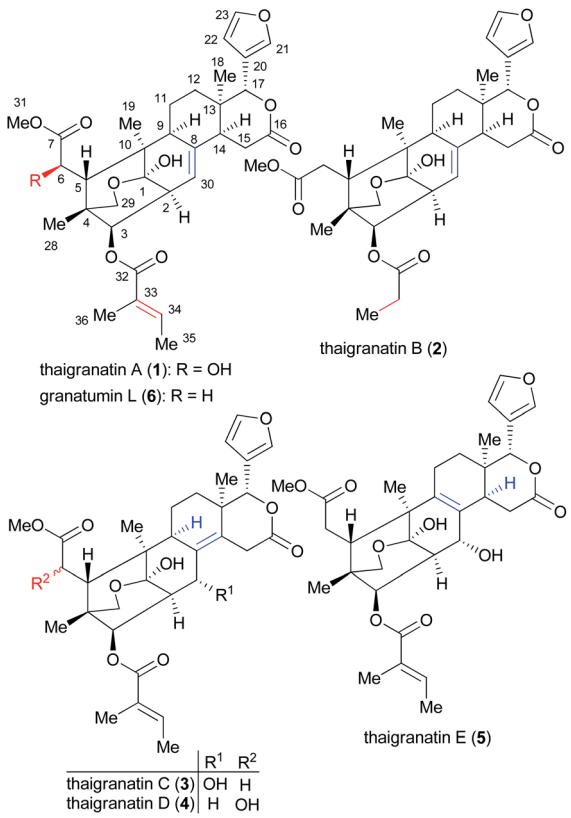

Fig. 2 Structures of thaigranatins A–E (**1–5**) and granatumin L (**6**) isolated from *Xylocarpus granatum*.[16]

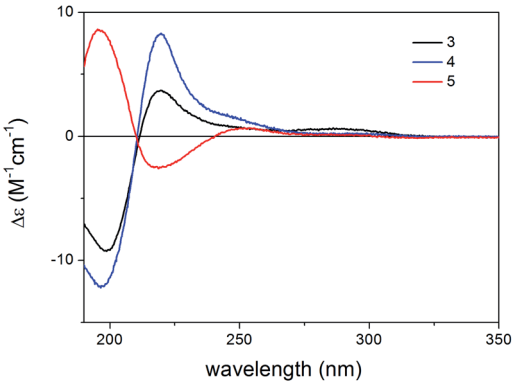

Fig. 3 Comparison of the experimental ECD spectra of **3–5** in MeCN.

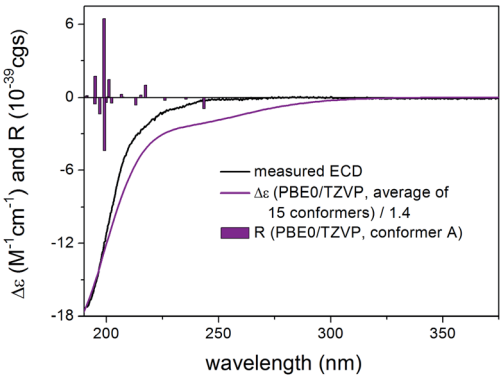

Fig. 4 Experimental ECD spectrum of **1** in MeCN compared with the Boltzmann-weighted PBE0/TZVP PCM/MeCN ECD spectrum of (1*R*,2*S*,3*R*,4*S*,5*S*,6*R*,9*S*,10*R*,13*R*,14*S*,17*R*)-**1**. Level of optimization: CAM-B3LYP/TZVP PCM/MeCN. Bars represent the rotatory strength values of the lowest-energy conformer. Experimental ECD spectrum of **1** was reproduced with permission from ref. 16.

work, we utilized TDDFT-ECD calculations of **1–6** with different combinations of methods to explain the ECD spectral differences of **1–6** and the mirror image ECD spectra of **3–5**. This approach was tested whether it is suitable to prove the proposed homochirality of **1–6** and thus it can provide an independent configurational assignment for **3–5**. Furthermore, the AC of C-6 in the side-chain of **4** remained undetermined.[16] In this work we applied DFT-NMR ^{13}C chemical shift calculations of the C-6 epimers to elucidate the AC of this chirality center.[27–29]

Semi-synthetic derivatives obtained by the derivatization of granatumin L (**6**) showed potent human immunodeficiency virus 1 (HIV-1) and influenza A virus (IAV) inhibitory activities, which may also justify to explore relationship between stereochemistry and characteristic ECD features and to determine solution geometries and confirm the absolute configuration.[16]

Results and discussion

Thaigranatin A (**1**) had a saturated δ-lactone chromophore with a C-17 furan-3-yl substituent, an α,β-unsaturated ester moiety (C-32 to C-35), an isolated ester (C-7) and a double bond ($\Delta^{8,30}$) chromophore. In the ECD spectrum of **1**, an intense negative ECD band could be observed below 200 nm with a flat negative plateau up to 270 nm. Since the absolute configuration was determined by single crystal X-ray diffraction analysis,[16] the ECD calculation of **1** was utilized to validate the applied DFT/TDDFT methods. The initial 29 Merck Molecular Force Field (MMFF) conformers of (1*R*,2*S*,3*R*,4*S*,5*S*,6*R*,9*S*,10*R*,13*R*,14*S*,17*R*)-**1** were re-optimized at the B3LYP/6-31+G(d,p), the CAM-B3LYP/TZVP[30,31] PCM/MeCN and the SOGGA11-X/TZVP[32,33] SMD/MeCN levels, separately. ECD spectra computed at various levels for the low-energy conformers over 1% Boltzmann population (15, 15 and 17 conformers, respectively) reproduced well the experimental ECD spectrum (Fig. 4). Since the CAM-B3LYP/TZVP PCM/MeCN and the SOGGA11-X/TZVP SMD/MeCN levels gave almost the same ECD results, only the first two levels were applied for the other derivatives in the DFT re-optimization step.

In all the CAM-B3LYP/TZVP PCM/MeCN conformers of **1**, the C-17 furan-3-yl group adopted an *equatorial* arrangement with *syn coplanar* orientation of the 17-H and C-21 atoms ($\omega_{17\text{-H,C-17,C-20,C-21}} = -10.2°$) and the 14-H had axial orientation. The δ-lactone ring had a distorted half-chair conformation with the C-13 being out of plane, while the other five atoms located in nearly one plane. The geometry of the low-energy conformers differed in the relative arrangements of the C-5 and C-3 substituents by rotation along the C-6 to C-7 and C-32 to C-33 sigma bonds (Fig. 5). In the lowest-energy conformer (conf A), the C-32 carbonyl oxygen was *syn coplanar* with the C-33 methyl

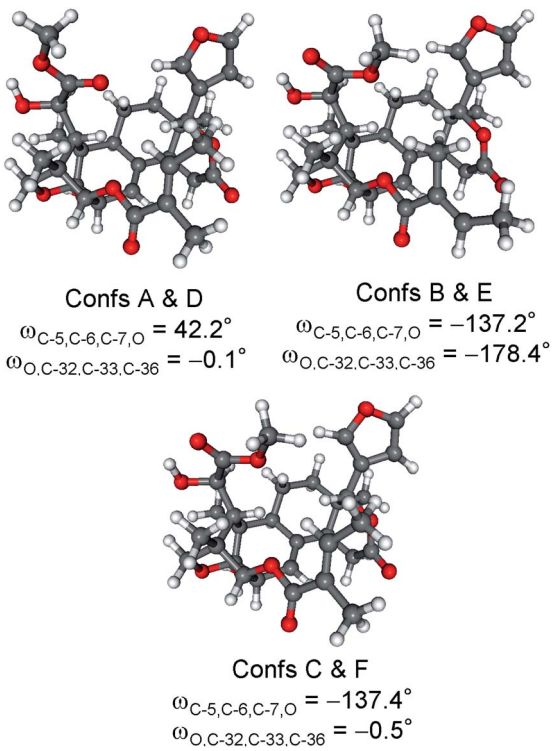

Fig. 5 Overlapped geometries and selected torsional angles of the six lowest-energy conformers of (1*R*,2*S*,3*R*,4*S*,5*S*,6*R*,9*S*,10*R*,13*R*,14*S*,17*R*)-**1**. Level of optimization: CAM-B3LYP/TZVP PCM/MeCN.

group ($\omega_{O=,C\text{-}32,C\text{-}33,C\text{-}36} = -0.1°$, s-*trans* conformation), while the C-5 had a *gauche* orientation with the C-7 carbonyl oxygen ($\omega_{C\text{-}5,C\text{-}6,C\text{-}7,=O} = 42.2°$). Conformers A and D differed only in the arrangements of the C-1 hydroxyl proton and they had identical computed ECD spectra (Fig. 6). Positive rotatory strength values were computed above 200 nm as shown in Fig. 4 but these were overcompensated by the negative ones. Conformers C and F had also positive computed transitions above 200 nm with larger intensity than those of conformers A and D manifesting in a positive CE (Fig. 6), and their geometries also differed only in the orientation of the 1-OH proton. Similarly to conformers A and D, conformers C and F had *syn coplanar* arrangement of the C-32 carbonyl oxygen (s-*trans* enone) and the C-33 methyl group but the C-5 had *gauche* orientation with the C-7 methoxy oxygen ($\omega_{C\text{-}5,C\text{-}6,C\text{-}7,=O} = -137.4°$). The positive CEs of conformers A, C, D, F were cancelled by the strong negative CEs of conformers B and E, in which the C-32 carbonyl oxygen was *anti periplanar* with the C-33 methyl group ($\omega_{O=,C\text{-}32,C\text{-}33,C\text{-}36} = -178.4°$, s-*cis* enone). Thus the rotation along the C-32 to C-33 bond of the α,β-unsaturated ester moiety and around the C-6 to C-7 bond was mostly responsible for the differences in the ECD spectra of the low-energy conformers of **1**.

Compared to compound **1**, **2** did not contain the conjugating $\Delta^{33,34}$ double bond and the C-6 chirality center in the other side chain and the experimental ECD spectrum had a strong negative CE below 210 nm and a weaker positive CE at 217 nm with a positive plateau up to 260 nm. Compound **2** had 43 initial MMFF conformers, the gas-phase and solvent model re-optimizations of which yielded 6 and 10 low-energy conformers over 1% Boltzmann-population. The first five low-energy CAM-B3LYP/TZVP PCM/MeCN conformers had differences in the orientation of the C-3 ester group and the furan ring while the lactone ring showed only marginal differences (Fig. 7). The individual computed ECDs of these conformers were similar but that of conformer E showed a significant red shift due to the opposite orientation of the furan ring (Fig. 8 and S2†). This red shift of the minor conformers obviously contributes to the high-wavelength positive shoulder of the experimental ECD spectrum. Similarly to the conformers of **1**, the δ-lactone ring had a distorted half-chair conformation in the low-energy conformers. The Boltzmann-weighted ECD spectra computed at all the applied combinations reproduced well the experimental spectrum including the positive CE and shoulder (Fig. 9), which confirmed the (1*R*,2*S*,3*R*,4*S*,5*S*,9*S*,10*R*,13*R*,14*S*,17*R*) absolute configuration of **2** and hence the homochirality with **1**.[16] The difference in the experimental ECD spectra of **1** and **2** can be attributed to the absence of the $\Delta^{33,34}$ double bond and the C-6 chirality center.

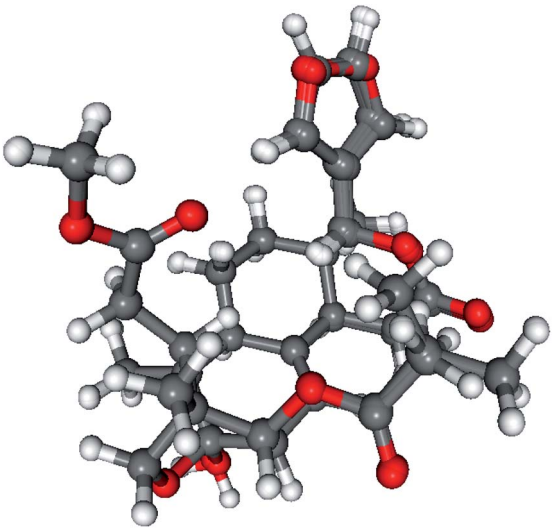

Fig. 7 Overlapped geometries of the five lowest-energy CAM-B3LYP/TZVP PCM/MeCN conformers of (1*R*,2*S*,3*R*,4*S*,5*S*,9*S*,10*R*,13*R*,14*S*,17*R*)-**2**.

Compound **3** contained the same C-3 α,β-unsaturated ester moiety as **1** but it missed the C-6 chirality center due to the exchange of the 6-OH group with a hydrogen atom. Moreover, the $\Delta^{8,30}$ double bond of **1** was shifted to $\Delta^{8,14}$ position in **3** and C-30 became a chirality center due to the presence of the *sec*-hydroxyl group. Besides the intense negative CE below 211 nm, the experimental ECD spectrum of **3** had a positive CE at

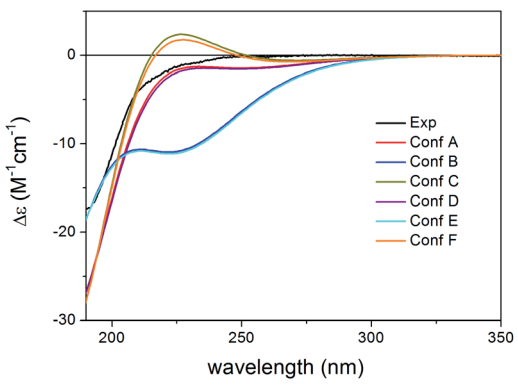

Fig. 6 Experimental ECD spectrum of **1** in MeCN compared with the PBE0/TZVP PCM/MeCN ECD spectra of the individual six lowest-energy CAM-B3LYP/TZVP PCM/MeCN conformers of (1*R*,2*S*,3*R*,4*S*,5*S*,6*R*,9*S*,10*R*,13*R*,14*S*,17*R*)-**1**.

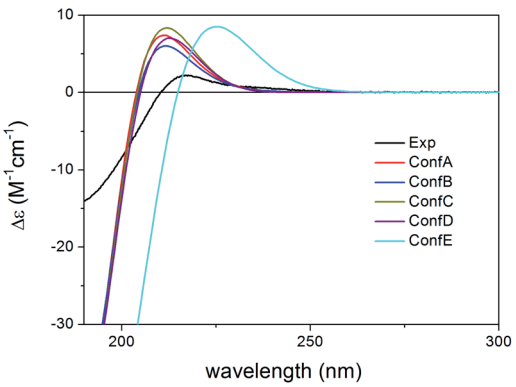

Fig. 8 Experimental ECD spectrum of **2** in MeCN compared with the B3LYP/TZVP PCM/MeCN ECD spectra of the individual five lowest-energy CAM-B3LYP/TZVP PCM/MeCN conformers of (1*R*,2*S*,3*R*,4*S*,5*S*,9*S*,10*R*,13*R*,14*S*,17*R*)-**2**. Experimental ECD spectrum of **2** was reproduced with permission from ref. 16.

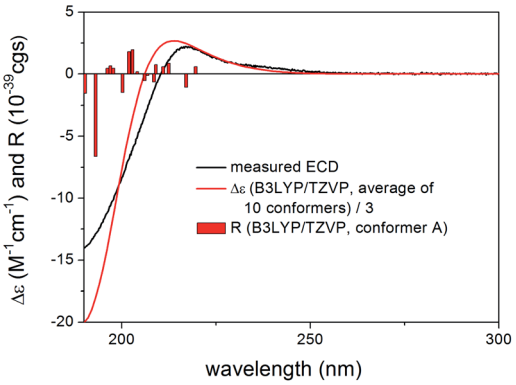

Fig. 9 Experimental ECD spectrum of **2** in MeCN compared with the Boltzmann-weighted B3LYP/TZVP PCM/MeCN ECD spectrum of (1*R*,2*S*,3*R*,4*S*,5*S*,9*S*,10*R*,13*R*,14*S*,17*R*)-**2**. Level of optimization: CAM-B3LYP/TZVP PCM/MeCN. Bars represent the rotatory strength values of the lowest-energy conformer.

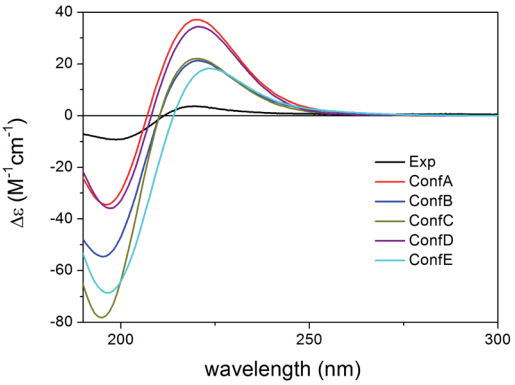

Fig. 11 Experimental ECD spectrum of **3** in MeCN compared with the B3LYP/TZVP PCM/MeCN ECD spectra of the individual five lowest-energy CAM-B3LYP/TZVP PCM/MeCN conformers of (1*R*,2*S*,3*R*,4*S*,5*S*,9*S*,10*R*,13*R*,17*R*,30*R*)-**3**.

220 nm accompanied with a flat positive shoulder having maximum at 286 nm.

Re-optimization of the initial 51 MMFF conformers of (1*R*,2*S*,3*R*,4*S*,5*S*,9*S*,10*R*,13*R*,17*R*,30*R*)-**3** resulted in 15 and 24 low-energy conformers over 1% Boltzmann-population in gas-phase and solvent model calculations, respectively. In the first five low-energy CAM-B3LYP/TZVP PCM/MeCN conformers, there were only minor difference in orientations of the two side-chains and the lactone ring (Fig. 10). Similarly to the lowest-energy conformer of **1**, the C-32 carbonyl oxygen of conformers A–E was *syn coplanar* with the C-33 methyl group ($\omega_{O=,C\text{-}32,C\text{-}33,C\text{-}36}$ = 34.8–37.8° range for confs A–E, *s-trans* enone) and the δ-lactone ring had a distorted half-chair conformation even with the sp^2-hybridized C-14. For the first five low-energy CAM-B3LYP/TZVP PCM/MeCN conformers, the computed ECD spectra had similar profile for the main transitions (Fig. 11). The different ECD profiles of compounds **1** and **3** derived from the different distributions of conformers differing in the C-3 side-chain conformation.

Boltzmann-weighted ECD spectra obtained at all combinations of the applied levels reproduced well the two major transitions at 220 and 199 nm while underestimated the positive shoulder at 286 nm (Fig. 12). Reproduction of the major transitions allowed verification of the absolute configuration of **3** as (1*R*,2*S*,3*R*,4*S*,5*S*,9*S*,10*R*,13*R*,17*R*,30*R*).

Similarly to compound **1**, **4** had a chirality center at C-6 and the only difference from **1** was the position of the $\Delta^{8,14}$ double bond. The absolute configuration of C-6 has not been determined independently in the original paper[16] thus we used TDDFT-ECD and ^{13}C NMR DFT calculations of the C-6 epimers to assign this chirality center.

Although chiroptical methods are usually applied for the elucidation of absolute configuration and conformation by exploiting the mirror image ECD profile of the enantiomers, there are reports where they were utilized successfully to distinguish diastereomers or more than two stereoisomers.[34–38] MMFF conformational search of the epimeric (1*R*,2*S*,3*R*,4*S*,5*S*,6*R*,9*S*,10*R*,13*R*,17*R*)-**4** and (1*R*,2*S*,3*R*,4*S*,5*S*,6*S*,9*S*,10*R*,13*R*,17*R*)-**4** produced 39 and 120 conformers, respectively, in a 21 kJ mol^{-1} energy window indicating considerable flexibility difference between the two

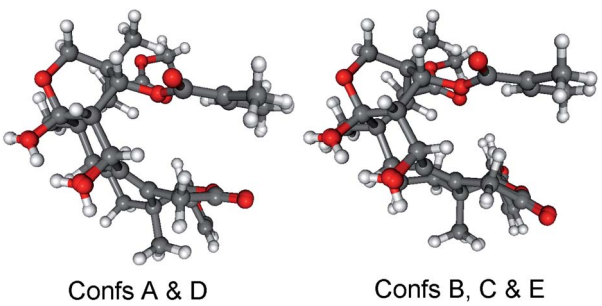

Fig. 10 Overlapped geometries of the five lowest-energy CAM-B3LYP/TZVP PCM/MeCN conformers of (1*R*,2*S*,3*R*,4*S*,5*S*,9*S*,10*R*,13*R*,17*R*,30*R*)-**3** (left: conformers A and D; right: conformers B, C and E).

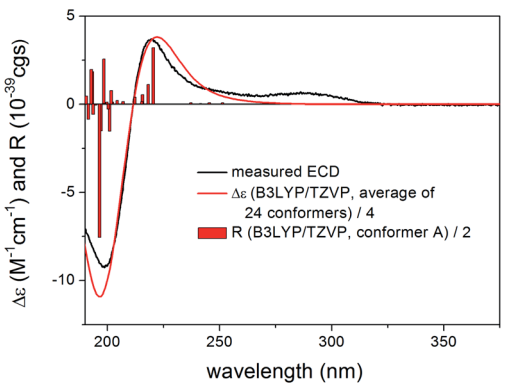

Fig. 12 Experimental ECD spectrum of **3** in MeCN compared with the Boltzmann-weighted B3LYP/TZVP PCM/MeCN ECD spectrum of (1*R*,2*S*,3*R*,4*S*,5*S*,9*S*,10*R*,13*R*,17*R*,30*R*)-**3**. Level of optimization: CAM-B3LYP/TZVP PCM/MeCN. Bars represent the rotatory strength values of the lowest-energy conformer.

diastereomers. After DFT re-optimization, ECD spectra were computed for 21/23 and 28/28 low-energy conformers in the gas-phase and the solvent-model calculations, respectively, and both epimers produced practically the same agreement with the experimental ECD (Fig. 13, S5 and S7†). This results allow verification of the absolute configuration of the core part as (1*R*,2*S*,3*R*,4*S*,5*S*,9*S*,10*R*,13*R*,17*R*) but it did not allow determining the AC of C-6. The C-3 substituent had s-*trans* conformation in most of the low-energy conformers (Fig. S4 and S6†). The configuration of the C-6 chirality center had apparently only minor contribution to the overall experimental ECD spectrum, and thus DFT ^{13}C NMR calculation was utilized to distinguish the epimers.

The DFT-NMR methods were validated first on compounds **1–3** and **6**. The widely applied mPW1PW91/6-311+G(2d,p)//B3LYP/6-31+G(d,p) level[27,39] was tested on **1–3** and **6** giving good agreement for most carbons (see ESI Tables S1–S4†). Then ^{13}C chemical shifts were computed for the epimeric (1*R*,2*S*,3*R*,4*S*,5*S*,6*R*,9*S*,10*R*,13*R*,17*R*)-**4** and (1*R*,2*S*,3*R*,4*S*,5*S*,6*S*,9*S*,10*R*,13*R*,17*R*)-**4**. The corrected mean absolute error (CMAE)[40] values were found rather similar (1.80 *vs.* 1.89) and the (6*R*) epimer appeared to be only slightly better in average (see Table S5†). A strong indication could be observed, however, for the C-5 carbon adjacent to the C-6 chirality center with more than 3 ppm difference suggesting (6*R*) configuration. Application of the DP4+ statistical method[41,42] gave a 95.23% confidence for the (6*R*) epimer which is above the empirical limit suggested by the developers[42] of the method for a solid determination of relative configuration.

In order to confirm further this result, the mPW1PW91/6-311+G(2d,p) SMD/$CHCl_3$//mPW1PW91/6-311+G(2d,p) SMD/$CHCl_3$ level[40] was also tested on **1**. This method including solvent model both at the DFT optimization and the NMR calculation step was not recommended by the CHESHIRE database,[43] since it was developed from a very limited test molecule set for a special case but we could apply it successfully lately for a different type of natural product together with the VCD and coupling constant results.[44] The solvent model NMR calculation of **1** gave similar results to those of the well-tested mPW1PW91/6-311+G(2d,p)//B3LYP/6-31+G(d,p) combination (see Table S6†). Thus it was also applied to the epimeric (1*R*,2*S*,3*R*,4*S*,5*S*,6*R*,9*S*,10*R*,13*R*,17*R*)-**4** and (1*R*,2*S*,3*R*,4*S*,5*S*,6*S*,9*S*,10*R*,13*R*,17*R*)-**4**. CMAE values obtained at this mPW1PW91/6-311+G(2d,p) SMD/$CHCl_3$//mPW1PW91/6-311+G(2d,p) SMD/$CHCl_3$ combination for the two epimers were found 1.69 for the (6*R*) and 1.96 for the (6*S*) diastereomer (see Table S7†). The DP4+ analysis showed a 99.81% confidence for the (6*R*) epimer. The two ^{13}C chemical shift DFT-NMR calculations produced the same conclusion for the AC of C-6 and together with the TDDFT-ECD calculations allowed elucidating the absolute configuration of **4** as (1*R*,2*S*,3*R*,4*S*,5*S*,6*R*,9*S*,10*R*,13*R*,17*R*).

The structure of compound **5** contained a $\Delta^{8,9}$ double bond instead of the $\Delta^{8,14}$ double bond of **3**, while their rings A–C had identical substitution pattern. Despite their closely related structures, compound **5** had oppositely signed CEs to the corresponding ones of **3** and **4**, which resulted in near mirror image experimental ECD spectra. The geometrical background for the mirror image ECD spectra of these homochiral derivatives was explored by TDDFT-ECD calculations.

Re-optimization of the 120 MMFF conformers of (1*R*,2*S*,3*R*,4*S*,5*S*,10*S*,13*R*,14*R*,17*R*,30*R*)-**5** yielded 19 and 25 low-energy conformers over 1% Boltzmann-population in the gas-phase and the solvent model calculations, respectively. In all the low-energy CAM-B3LYP/TZVP PCM/MeCN conformers, the δ-lactone ring adopted a distorted boat conformation with C-15 and C-17 being out of plane (Fig. 14). This conformation of the δ-lactone ring was different from the preferred half-chair conformation of **1–4**, and it was the reason of the mirror image ECD curves. The ECD spectra computed for the low-energy CAM-B3LYP/TZVP PCM/MeCN conformers reproduced well the experimental ECD curve of **5** (Fig. 15 and S10†), which confirmed that the geometries of the conformers were predicted properly. Interestingly, the B3LYP/6-31+G(d,p) gas-phase re-optimization provided different low-energy conformers, in

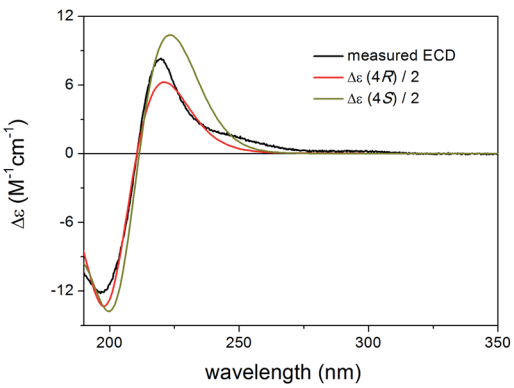

Fig. 13 Experimental ECD spectrum of **4** in MeCN compared with the Boltzmann-weighted B3LYP/TZVP PCM/MeCN ECD spectrum of (1*R*,2*S*,3*R*,4*S*,5*S*,6*R*,9*S*,10*R*,13*R*,17*R*)-**4** (average of 23 conformers) and the Boltzmann-weighted CAM-B3LYP/TZVP PCM/MeCN ECD spectrum of (1*R*,2*S*,3*R*,4*S*,5*S*,6*S*,9*S*,10*R*,13*R*,17*R*)-**4** (average of 28 conformers). Level of optimization: CAM-B3LYP/TZVP PCM/MeCN.

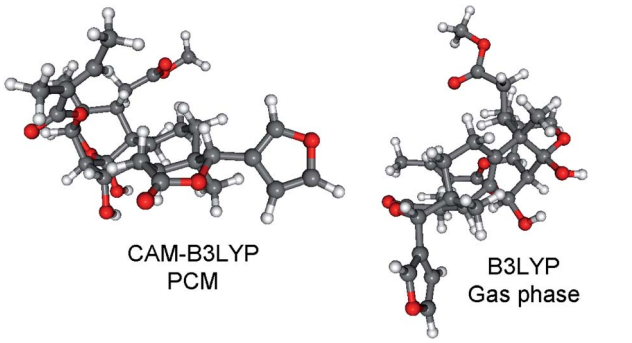

Fig. 14 Comparison of the lowest-energy CAM-B3LYP/TZVP PCM/MeCN (12.7%) and B3LYP/6-31+G(d,p) gas-phase (10.8%) conformers of (1*R*,2*S*,3*R*,4*S*,5*S*,10*S*,13*R*,14*R*,17*R*,30*R*)-**5**.

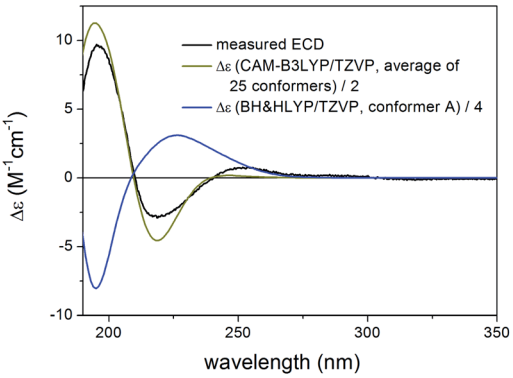

Fig. 15 Experimental ECD spectrum of **5** in MeCN compared with the Boltzmann-weighted CAM-B3LYP/TZVP PCM/MeCN ECD spectrum of (1*R*,2*S*,3*R*,4*S*,5*S*,10*S*,13*R*,14*R*,17*R*,30*R*)-**5** (level of optimization: CAM-B3LYP/TZVP PCM/MeCN) and the lowest-energy BH&HLYP/TZVP ECD spectrum of (1*R*,2*S*,3*R*,4*S*,5*S*,10*S*,13*R*,14*R*,17*R*,30*R*)-**5** [level of optimization: B3LYP/6-31+G(d,p)].

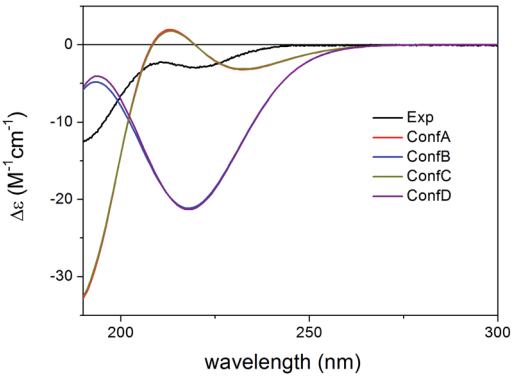

Fig. 17 Experimental ECD spectrum of **6** in MeCN compared with the BH&HLYP/TZVP PCM/MeCN ECD spectra of the individual four lowest-energy CAM-B3LYP/TZVP PCM/MeCN conformers of (1*R*,2*S*,3*R*,4*S*,5*S*,9*S*,10*R*,13*R*,14*S*,17*R*)-**6**. Experimental ECD spectrum of **6** was reproduced with permission from ref. 16.

which the δ-lactone ring had the half-chair conformation (Fig. 14) and the computed ECD gave mirror image agreement with the two high-energy ECD transitions (Fig. 15 and S11†). This result confirmed that the shift of the position of the double bond in **3** and **5** (from $\Delta^{8,14}$ to $\Delta^{8,9}$) changed the preferred conformation of the δ-lactone ring from half-chair to boat, which is manifested in near mirror ECD spectra, while the corresponding chirality centers had identical absolute configuration.

This is an instructive example how chiroptical properties of structurally related compounds can differ and why it is important to apply more than one functional in both the DFT optimization and the ECD calculation steps.[1,2,45,46] The solvent model results reproduced the experimental ECD spectrum allowing verification of the homochiral nature of **5** with the AC of (1*R*,2*S*,3*R*,4*S*,5*S*,10*S*,13*R*,14*R*,17*R*,30*R*) despite its nearly mirror image experimental ECD.

Compared to the structure of **1**, compound **6** does not contain the C-6 chirality center and since this center does not have significant contribution to the ECD spectrum, the experimental ECD spectra of **1** and **6** were very similar. The initial 34 MMFF conformers of (1*R*,2*S*,3*R*,4*S*,5*S*,9*S*,10*R*,13*R*,14*S*,17*R*)-**6** were re-optimized at the B3LYP/6-31+G(d,p) and the CAM-B3LYP/TZVP PCM/MeCN levels resulting in 4 and 12 low-energy conformers, respectively. The δ-lactone ring adopted half-chair conformation in all the low-energy CAM-B3LYP/TZVP PCM/MeCN conformers of **6**, while the α,β-unsaturated ester moiety had s-*trans* conformation in conformers A and C and s-*cis* in conformers B and D (Fig. 16). The computed ECD spectra of conformers A and C had a weak positive CE at 220 nm, which did not match the experimental curve (Fig. 17). However, the intense negative computed ECD bands of conformers B and D below 225 nm overrode the positive CE of conformers A and C.[14] The negative CEs of the experimental ECD spectra below 220 nm are mainly determined by the contribution of the higher-energy conformers B and D containing an s-*cis* enone chromophore.

All combinations of the applied levels reproduced nicely the experimental ECD spectrum (Fig. 18) allowing verification of the

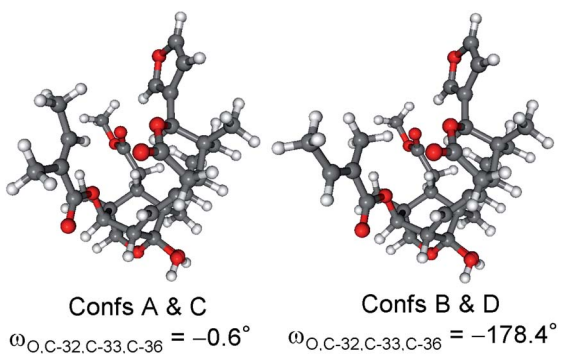

Fig. 16 Overlapped geometries and selected torsional angle of the four lowest-energy conformers of (1*R*,2*S*,3*R*,4*S*,5*S*,9*S*,10*R*,13*R*,14*S*,17*R*)-**6**. Level of optimization: CAM-B3LYP/TZVP PCM/MeCN.

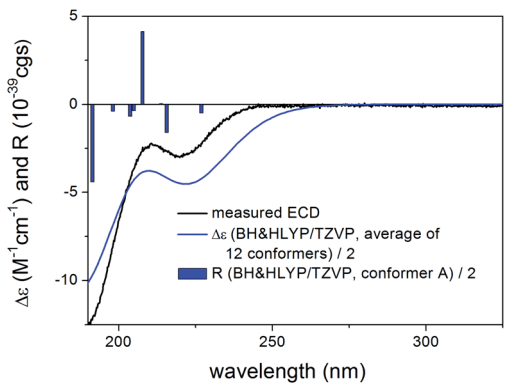

Fig. 18 Experimental ECD spectrum of **6** in MeCN compared with the Boltzmann-weighted BH&HLYP/TZVP PCM/MeCN ECD spectrum of (1*R*,2*S*,3*R*,4*S*,5*S*,9*S*,10*R*,13*R*,14*S*,17*R*)-**6**. Level of optimization: CAM-B3LYP/TZVP PCM/MeCN. Bars represent the rotatory strength values of the lowest-energy conformer.

homochiral (1*R*,2*S*,3*R*,4*S*,5*S*,9*S*,10*R*,13*R*,14*S*,17*R*) AC proposed on the similarity of the experimental ECD spectra of **1** and **6**.[16]

Conclusions

TDDFT-ECD calculations of homochiral derivatives **1–6** with different combinations of methods could explain differences in the experimental ECD spectra, and geometries of structural subunits could be correlated with characteristic ECD profiles. The calculations revealed that the boat conformation of the δ-lactone ring of **5** was responsible for the near mirror ECD spectra compared to those of **3** and **4**, the low-energy conformers of which had half-chair conformation for the δ-lactone ring. The different conformations were induced by different positions of the double bond ($\Delta^{8,14}$ or $\Delta^{8,9}$) in **3–5**. The s-*cis* or s-*trans* conformation of the planar α,β-unsaturated ester chromophore was found responsible for spectral differences in **1–4** and **6**, while the C-5 ester substituent and C-6 chirality center did not have significant contribution. The (6*R*) AC of thaigranatin D (**4**) could be determined by the ^{13}C NMR chemical shift calculations of the C-6 epimers by two methods. The results may contribute to understand better the geometrical parameters governing the ECD spectra of these limonoids and thus to use ECD more efficiently for their stereochemical analysis.

Experimental

General information

Isolation and characterization of **1–6** was described in ref. 15 and 16. ECD spectra were measured on a Jasco J-810 spectropolarimeter (JASCO Corporation, Tokyo, Japan) in MeCN.

Computational section

Mixed torsional/low-frequency mode conformational searches were carried out by means of the Macromodel 10.8.011 software by using the Merck Molecular Force Field (MMFF) with an implicit solvent model for $CHCl_3$.[47] Geometry reoptimizations were carried out at the B3LYP/6-31+G(d,p) level *in vacuo*, the CAM-B3LYP/TZVP level with the PCM solvent model for MeCN, the mPW1PW91/6-311+G(2d,p)[39] SMD/$CHCl_3$ and the SOGGA11-X/TZVP SMD/MeCN levels. TDDFT-ECD calculations were run with various functionals (B3LYP, BH&HLYP, CAM-B3LYP, and PBE0) and the TZVP basis set as implemented in the Gaussian 09 package with the same or no solvent model as in the preceding DFT optimization step.[48] ECD spectra were generated as sums of Gaussians with 3000–6000 cm^{-1} width at half-height, using dipole-velocity-computed rotational strength values.[49] NMR calculations were performed at the mPW1PW91/6-311+G(2d,p) and the mPW1PW91/6-311+G(2d,p) SMD/$CHCl_3$ levels on the B3LYP/6-31+G(d,p) and the mPW1PW91/6-311+G(2d,p) SMD/$CHCl_3$ levels, respectively. Computed NMR shift data were corrected with $I = 185.4855$ and $S = -1.0306$ in the gas-phase[27] and $I = 187.9864$ and $S = -1.0358$ in the solvent model calculations.[40] Boltzmann distributions were estimated from the B3LYP, CAM-B3LYP, mPW1PW91 and SOGGA11-X energies. The MOLEKEL software package was used for visualization of the results.[50]

Conflicts of interest

There are no conflicts to declare.

Acknowledgements

The research was supported by the EU and cofinanced by the European Regional Development Fund under the project GINOP-2.3.2-15-2016-00008. T. K. thanks the National Research, Development and Innovation Office (K120181) and A. M. the János Bolyai Research Scholarship of the Hungarian Academy of Sciences and the ÚNKP-19-4 New National Excellence Program of the Ministry for Innovation and Technology. The Governmental Information-Technology Development Agency (KIFÜ) is acknowledged for CPU time.

Notes and references

1 S. Superchi, P. Scafato, M. Górecki and G. Pescitelli, *Curr. Med. Chem.*, 2018, **25**, 287–320.
2 A. Mándi and T. Kurtán, *Nat. Prod. Rep.*, 2019, **36**, 889–918.
3 L. Grauso, R. Teta, G. Esposito, M. Menna and A. Mangoni, *Nat. Prod. Rep.*, 2019, **36**, 1005–1030.
4 I. Kock, S. Draeger, B. Schulz, B. Elsässer, T. Kurtán, Á. Kenéz, S. Antus, G. Pescitelli, P. Salvadori, J. B. Speakman, J. Rheinheimer and K. Krohn, *Eur. J. Org. Chem.*, 2009, **2009**, 1427–1434.
5 P. Moosmann, R. Ueoka, L. Grauso, A. Mangoni, B. I. Morinaka, M. Gugger and J. Piel, *Angew. Chem., Int. Ed.*, 2017, **56**, 4987–4990.
6 C. Y. An, X. M. Li, H. Luo, C. S. Li, M. H. Wang, G. M. Xu and B. G. Wang, *J. Nat. Prod.*, 2013, **76**, 1896–1901.
7 D. H. El-Kashef, G. Daletos, M. Plenker, R. Hartmann, A. Mándi, T. Kurtán, H. Weber, W. Lin, E. Ancheeva and P. Proksch, *J. Nat. Prod.*, 2019, **82**, 2460–2469.
8 J. E. Rode, M. Górecki, S. Witkowski and J. Frelek, *Phys. Chem. Chem. Phys.*, 2018, **20**, 22525–22536.
9 S. Kun, N. Kánya, N. Galó, A. Páhi, A. Mándi, T. Kurtán, P. Makleit, Sz. Veres, Á. Sipos, T. Docsa and L. Somsák, *J. Agric. Food Chem.*, 2019, **67**, 6884–6891.
10 H. Zhou, L. Li, C. Wu, T. Kurtán, A. Mándi, Y. Liu, Q. Gu, T. Zhu, P. Guo and D. Li, *J. Nat. Prod.*, 2016, **79**, 1783–1790.
11 S. McLean, *Can. J. Chem.*, 1964, **42**, 191–195.
12 W. Klyne and W. M. Stokes, *J. Chem. Soc.*, 1954, 1979–1988.
13 Y. Z. Sun, T. Kurtán, A. Mándi, H. Tang, Y. Chou, K. Soong, L. Su, P. Sun, C. L. Zhuang and W. Zhang, *J. Nat. Prod.*, 2017, **80**, 2930–2940.
14 A. Mándi, I. W. Mudianta, T. Kurtán and M. J. Garson, *J. Nat. Prod.*, 2015, **78**, 2051–2056.
15 M. Y. Li, Q. Xiao, T. Satyanandamurty and J. Wu, *Chem. Biodiversity*, 2014, **11**, 262–275.
16 J. L. Ren, X. P. Zou, W. S. Li, L. Shen and J. Wu, *Mar. Drugs*, 2018, **16**, 434.

17 R. X. Liu, Q. Liao, L. Shen and J. Wu, *Fitoterapia*, 2018, **131**, 96–104.
18 Y. B. Wu, Y. Z. Wang, Z. Y. Ni, X. Qing, Q. W. Shi, F. Sauriol, C. J. Vavricka, Y. C. Gu and H. Kiyota, *J. Nat. Prod.*, 2017, **80**, 2547–2550.
19 M. Liao, P. Pedpradab and J. Wu, *Phytochem. Lett.*, 2017, **19**, 126–131.
20 Z. F. Zhou, T. Kurtán, A. Mándi, Y. C. Gu, L. G. Yao, G. R. Xin, X. W. Li and Y. W. Guo, *Sci. Rep.*, 2016, **6**, 33908.
21 J. Li, M. Y. Li, G. Feng, J. Zhang, M. Karonen, J. Sinkkonen, T. Satyanandamurty and J. Wu, *J. Nat. Prod.*, 2012, **75**, 1277–1283.
22 J. Li, M. Y. Li, T. Satyanandamurty and J. Wu, *Helv. Chim. Acta*, 2011, **94**, 1651–1656.
23 I. A. Najmuldeen, A. H. A. Hadi, K. Awang, K. Mohamad, K. A. Ketuly, M. R. Mukhtar, S. L. Chong, G. Chan, M. A. Nafiah, N. S. Weng, O. Shirota, T. Hosoya, A. E. Nugroho and H. Morita, *J. Nat. Prod.*, 2011, **74**, 1313–1317.
24 K. Awang, C. S. Lim, K. Mohamad, H. Morita, Y. Hirasawa, K. Takeya, O. Thoison and A. H. A. Hadi, *Bioorg. Med. Chem.*, 2007, **15**, 5997–6002.
25 S. Vardhan and S. K. Sahoo, *Comput. Biol. Med.*, 2020, **124**, 103936.
26 S. Fu and B. Liu, *Org. Chem. Front.*, 2020, **7**, 1903–1947.
27 M. W. Lodewyk, M. R. Siebert and D. J. Tantillo, *Chem. Rev.*, 2012, **112**, 1839–1862.
28 Y. M. Ren, C. Q. Ke, A. Mándi, T. Kurtán, C. Tang, S. Yao and Y. Ye, *Tetrahedron*, 2017, **73**, 3213–3219.
29 M. Kicsák, A. Mándi, Sz. Varga, M. Herczeg, Gy. Batta, A. Bényei, A. Borbás and P. Herczegh, *Org. Biomol. Chem.*, 2018, **16**, 393–401.
30 T. Yanai, D. Tew and N. Handy, *Chem. Phys. Lett.*, 2004, **393**, 51–57.
31 G. Pescitelli, L. di Bari and N. Berova, *Chem. Soc. Rev.*, 2011, **40**, 4603–4625.
32 R. Peverati and D. G. Truhlar, *J. Chem. Phys.*, 2011, **135**, 191102.
33 É. Brémond, M. Savarese, N. Q. Su, Á. J. Pérez-Jiménez, X. Xu, J. C. Sancho-García and C. Adamo, *J. Chem. Theory Comput.*, 2016, **12**, 459–465.
34 E. Ancheeva, L. Küppers, S. H. Akone, W. Ebrahim, Z. Liu, A. Mándi, T. Kurtán, W. Lin, R. Orfali, N. Rehberg, R. Kalscheuer, G. Daletos and P. Proksch, *Eur. J. Org. Chem.*, 2017, **2017**, 3256–3264.
35 Y. Liu, T. Kurtán, A. Mándi, H. Weber, C. Wang, R. Hartmann, W. Lin, G. Daletos and P. Proksch, *Tetrahedron Lett.*, 2018, **59**, 632–636.
36 P. Zhang, L. H. Meng, A. Mándi, T. Kurtán, X. M. Li, Y. Liu, X. Li, C. S. Li and B. G. Wang, *Eur. J. Org. Chem.*, 2014, **2014**, 4029–4036.
37 L. F. Liang, T. Kurtán, A. Mándi, L. G. Yao, J. Li, L. F. Lan and Y. W. Guo, *Tetrahedron*, 2018, **74**, 1933–1941.
38 J. L. Johnson, D. S. Nair, S. M. Pillai, D. Johnson, Z. Kallingathodi, I. Ibnusaud and P. L. Polavarapu, *ACS Omega*, 2019, **4**, 6154–6164.
39 C. Adamo and V. Barone, *J. Chem. Phys.*, 1998, **108**, 664–675.
40 S. Qiu, E. de Gussem, K. A. Tehrani, S. Sergeyev, P. Bultinck and W. Herrebout, *J. Med. Chem.*, 2013, **56**, 8903–8914.
41 S. G. Smith and J. M. Goodman, *J. Am. Chem. Soc.*, 2010, **132**, 12946–12959.
42 N. Grimblat, M. M. Zanardi and A. M. Sarotti, *J. Org. Chem.*, 2015, **80**, 12526–12534.
43 CHESHIRE CCAT, *The Chemical Shift Repository for computed NMR scaling factors*, http://cheshirenmr.info/index.htm.
44 N. M. Tran-Cong, A. Mándi, T. Kurtán, W. E. G. Müller, R. Kalscheuer, W. Lin, Z. Liu and P. Proksch, *RSC Adv.*, 2019, **9**, 27279–27288.
45 P. Sun, D. X. Xu, A. Mándi, T. Kurtán, T. J. Li, B. Schulz and W. Zhang, *J. Org. Chem.*, 2013, **78**, 7030–7047.
46 V. F. Ximenes, N. H. Morgon and A. R. de Souza, *Chirality*, 2018, **30**, 1049–1053.
47 MacroModel. Schrödinger LLC, 2015. http://www.schrodinger.com/MacroModel.
48 M. J. Frisch, G. W. Trucks, H. B. Schlegel, G. E. Scuseria, M. A. Robb, J. R. Cheeseman, G. Scalmani, V. Barone, B. Mennucci, G. A. Petersson, H. Nakatsuji, M. Caricato, X. Li, H. P. Hratchian, A. F. Izmaylov, J. Bloino, G. Zheng, J. L. Sonnenberg, M. Hada, M. Ehara, K. Toyota, R. Fukuda, J. Hasegawa, M. Ishida, T. Nakajima, Y. Honda, O. Kitao, H. Nakai, T. Vreven, J. A. Montgomery Jr, J. E. Peralta, F. Ogliaro, M. Bearpark, J. J. Heyd, E. Brothers, K. N. Kudin, V. N. Staroverov, R. Kobayashi, J. Normand, K. Raghavachari, A. Rendell, J. C. Burant, S. S. Iyengar, J. Tomasi, M. Cossi, N. Rega, J. M. Millam, M. Klene, J. E. Knox, J. B. Cross, V. Bakken, C. Adamo, J. Jaramillo, R. Gomperts, R. E. Stratmann, O. Yazyev, A. J. Austin, R. Cammi, C. Pomelli, J. W. Ochterski, R. L. Martin, K. Morokuma, V. G. Zakrzewski, G. A. Voth, P. Salvador, J. J. Dannenberg, S. Dapprich, A. D. Daniels, Ö. Farkas, J. B. Foresman, J. V. Ortiz, J. Cioslowski and D. J. Fox, *Gaussian 09 (Revision E.01)*, Gaussian, Inc., Wallingford, CT, 2013.
49 P. J. Stephens and N. Harada, *Chirality*, 2010, **22**, 229–233.
50 U. Varetto, *MOLEKEL 5.4*, Swiss National Supercomputing Centre, Manno, Switzerland, 2009.

